Proceedings of the ASME 2010 3rd Joint US-European Fluids Engineering Summer Meeting and 8th International Conference on Nanochannels, Microchannels, and Minichannels
FEDSM-ICNMM2010
August 1-5, 2010, Montreal, Canada

FEDSM-ICNMM2010-30634

A COMBINED SOFT-SPHERE COLLISION / IMMERSED BOUNDARY METHOD FOR RESOLVED SIMULATIONS OF PARTICULATE FLOWS

Wim-Paul Breugem*
Laboratory for Aero & Hydrodynamics
Delft University of Technology
Leeghwaterstraat 21, 2628 CA Delft, The Netherlands
Email: w.p.breugem@tudelft.nl

ABSTRACT

A second-order accurate and efficient Immersed Boundary Method (IBM) has been developed for simulating particle-laden flows. Recently, this method has been combined with a soft-sphere collision model to accommodate inter-particle and particle-wall collisions. Details of the collision model are given. Results are shown from a lubrication study of non-touching particles at close distance from each other. The numerical results for the drag force acting on the particles agree well with exact solutions, except when the gap width between the particles becomes significantly smaller than the numerical grid spacing. For very small gap width, lubrication force corrections are proposed for the normal approach between particles based on asymptotic analytical solutions. Results are presented from a numerical study of sphere-wall collisions in a viscous fluid. The simulated behavior of the coefficient of restitution as function of the Stokes number based on the particle impact velocity, is in good agreement with experimental data.

NOMENCLATURE

e coefficient of restitution
e_d dry coefficient of restitution
$\underline{f}^{n+1/2}$ IBM force at time level $n+1/2$
$\underline{g}$ gravitational acceleration
k_n normal spring stiffness
m_e effective mass of two colliding particles
$\underline{n}$ outward unit normal on surface particle
p fluid pressure
$\tilde{p}$ correction pressure
$\underline{r}$ diffusion minus advection term
t time
$\underline{u}$ fluid velocity
$\underline{u}_c$ centroid velocity of particle
$\underline{u}^*$ first prediction velocity
$\underline{u}^{**}$ second prediction velocity
$\underline{x}_c$ position vector of particle centroid
$\underline{x}_{ijk}$ position vector of Eulerian grid point (i,j,k)
A surface area
$\underline{F}_{ab,n}$ normal collision force between particles a and b
H Heaviside step function
$\underline{\underline{I}}$ unit tensor
I_c moment of inertia of (spherical) particle
N_c number of computational time steps in collision
N_q number of iterations in multi-direct forcing scheme
R radius of sphere
Re_c particle Reynolds number
St Stokes number
$\underline{U}_d$ particle (segment) velocity
V_c volume of particle
V_l volume of Lagrangian grid cell with index l
$\underline{X}$ position vector of particle segment
$\underline{X}_l$ position vector of Lagrangian grid point l
∂V surface of particle
α_{ijk} solid volume fraction of Eulerian grid cell (i,j,k)

*Address all correspondence to this author.

δ_d regularized Dirac delta function
δ_n normal overlap distance
ε gap width normalized by sphere radius
η_n normal damping coefficient
λ Stokes amplification factor
μ_f dynamic viscosity of fluid
ν_f kinematic viscosity of fluid
ρ_f mass density of fluid
ρ_p mass density of particle
$\underline{\underline{\tau}}$ fluid stress tensor
ϕ signed distance to particle surface (level-set function)
$\underline{\omega}_c$ angular velocity of particle
Δt computational time step
Δx computational grid spacing of Eulerian grid
$\Delta \underline{F}$ lubrication force correction
ΔV_l volume of Lagrangian grid cell

1. INTRODUCTION

Particle-laden / particulate flows are found in many applications ranging from fluidized bed reactors in the chemical industry, transport of sediment by rivers and streams, sedimentation processes in a hopper dredger and flocculation/sedimentation processes in the treatment of drinking water. The fundamental understanding of such flows is still rather poor, in particular when the solid volume fraction is not small. Fundamental issues of interest are the modulation of turbulence by the presence of particles and preferential concentration / particle clustering. Numerical simulations become expensive when particles are larger than the Kolmogorov scale and the flow in the immediate vicinity of a particle needs to be resolved.

The work presented in this paper is part of a research project with the aim to develop a parallel Direct Numerical Simulation (DNS) code for simulating $O\left(10^3\right)$ finite-size particles in turbulent flows. For the particle-fluid coupling a modified version [1] of the efficient Immersed Boundary Method (IBM) of Uhlmann [2] has been developed. Recently, this model has been extended with a soft-sphere collision model [3] to accurately represent inter-particle and particle-wall interactions. In this paper the combined IBM / soft-sphere collision model is explained. Results are shown from a lubrication study of the hydrodynamic interaction between non-touching particles at close distance from each other and from a study of sphere-wall collisions in a viscous fluid.

The structure of this paper is as follows. In section 2 the governing equations are given for the fluid phase and for the particles. In section 3 and 4 the IBM used for the particle-fluid coupling is explained. In section 5 the soft-sphere collision model is explained. Details of the numerical implementation are given in section 6. In section 7 results are shown from the lubrication study. In section 8 results are presented from the study of sphere-wall collisions. Finally, in section 9 the main conclusions are summarized.

2. GOVERNING EQUATIONS

The fluid phase of particulate flows is described by the incompressible Navier-Stokes equations, which read:

$$\nabla \cdot \underline{u} = 0\,, \tag{1a}$$

$$\frac{\partial \underline{u}}{\partial t} + \nabla \cdot \underline{u}\,\underline{u} = -\frac{1}{\rho_f}\nabla p + \nu_f \nabla^2 \underline{u}\,, \tag{1b}$$

where $\underline{u}$ is the velocity, p is the modified pressure (i.e., the pressure minus the hydrostatic contribution), ρ_f is the mass density of the fluid and ν_f is the kinematic fluid viscosity that is equal to μ_f/ρ_f with μ_f the dynamic fluid viscosity.

The velocity $\underline{U}_d$ of a particle segment at position $\underline{X}$ can be decomposed into a translational part and a rotational part according to:

$$\underline{U}_d\left(\underline{X}\right) = \underline{u}_c + \underline{\omega}_c \times \left(\underline{X} - \underline{x}_c\right)\,, \tag{2}$$

where $\underline{u}_c$ is the velocity of the particle centroid at $\underline{X} = \underline{x}_c$ and $\underline{\omega}_c$ is the angular velocity of the particle. In this paper only results are shown for solid spheres. The time evolution of the centroid and angular velocities is governed by the Newton-Euler equations, which for a sphere can be written as:

$$\rho_p V_c \frac{d\underline{u}_c}{dt} = \rho_f \oint_{\partial V} \underline{\underline{\tau}} \cdot \underline{n}\, dA + \left(\rho_p - \rho_f\right) V_c \underline{g}\,, \tag{3a}$$

$$I_c \frac{d\underline{\omega}_c}{dt} = \rho_f \oint_{\partial V} \left(\underline{X} - \underline{x}_c\right) \times \left(\underline{\underline{\tau}} \cdot \underline{n}\right) dA\,. \tag{3b}$$

Here ρ_p is the mass density of the sphere, $V_c = (4/3)\pi R^3$ is the volume of a sphere with radius R, $\underline{\underline{\tau}} = -p\underline{\underline{I}} + \mu_f\left(\nabla \underline{u} + \nabla \underline{u}^T\right)$ is the fluid stress tensor with $\underline{\underline{I}}$ the unit tensor, $\underline{n}$ is the outward unit normal at the surface ∂V of the sphere, $\underline{g}$ is the gravitational acceleration and $I_c = (2/5)\rho_p V_c R^2$ is the moment of inertia of a solid sphere. Note that in Eqn. (3a) the term $-\rho_f V_c \underline{g}$ is included to account for the buoyant force from the background hydrostatic pressure stratification.

Eqns (1a)-(1b) and (3a)-(3b) are coupled and have to be solved together with the no-slip / no-penetration conditions at the surface of the solid particles ($\underline{u} = \underline{U}_d$ at ∂V).

3. IMMERSED BOUNDARY METHOD

The principle of the IBM is that the Navier-Stokes equations (1a)-(1b) are not only solved in the fluid phase, but in the entire domain, *including* the space occupied by the particles. In the immediate vicinity of the surface of the solid particles an *extra* force is added to the right-hand side of the momentum equation

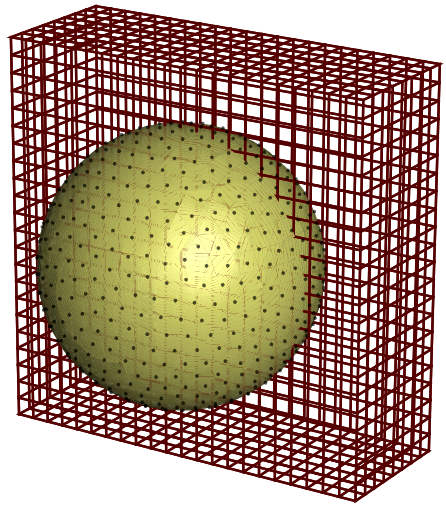

FIGURE 1. EULERIAN GRID AND THE DISTRIBUTION OF THE LAGRANGIAN GRID POINTS OVER A SPHERE FOR $2R/\Delta x = 16$ AND RETRACTION OF $0.3\Delta x$. THE NUMBER OF LAGRANGIAN GRID POINTS ON THE (RETRACTED) SURFACE OF THE SPHERE IS EQUAL TO 746.

(1b) such that *by good approximation* $\underline{u} \approx \underline{U}_d$ at ∂V. Thus, the no-slip / no-penetration conditions at the particle-fluid interface are not imposed directly as in conventional methods employing body-conforming grids, but indirectly by means of adding forces to the flow field near the surface of a particle. The main advantage is that a fixed, continuous and structured grid can be used for the fluid phase for which computationally efficient methods are available. Another advantage of the IBM is that it does not require regridding in case of *moving* particles.

When using IBMs the price that has to be paid is some loss in the accuracy. The challenge is to develop a method that is not only efficient, but also sufficiently accurate at the same time. Throughout the years numerous variants of the IBM have been developed and successfully applied to many different flow problems. A recent review of the IBM is given by Mittal and Iaccarino [4].

Recently, Uhlmann [2] developed an efficient IBM for simulating particulate flows. The method makes use of two different grids as illustrated in Fig. 1. A uniform, staggered Cartesian grid is used for the fluid phase, to which I will refer to as the *Eulerian* grid. Furthermore, the method makes use of a uniform *Lagrangian* grid that is attached to and moves with the surface of the particles.

The IBM of Uhlmann is integrated in a pressure-correction method, which for clarity is given here in semi-discrete form and based on the Crank-Nicolson scheme for time integration:

$$\underline{u}^* = \underline{u}^n + \Delta t \left(-\frac{1}{\rho_f} \nabla p^{n-1/2} + \underline{r}^{n+1/2} \right), \tag{4a}$$

$$\underline{u}^{**} = \underline{u}^* + \Delta t \, \underline{f}^{n+1/2}, \tag{4b}$$

$$\frac{1}{\rho_f} \nabla^2 \tilde{p} = \frac{1}{\Delta t} \nabla \cdot \underline{u}^{**}, \tag{4c}$$

$$\underline{u}^{n+1} = \underline{u}^{**} - \frac{\Delta t}{\rho_f} \nabla \tilde{p}, \tag{4d}$$

$$p^{n+1/2} = p^{n-1/2} + \tilde{p}, \tag{4e}$$

where $\underline{r} \equiv -\nabla \cdot \underline{u}\,\underline{u} + \nu_f \nabla^2 \underline{u}$, $\underline{u}^*$ is the first prediction velocity, $\underline{u}^{**}$ is the second prediction velocity that includes the forcing from the IBM, $\tilde{p}$ is the correction pressure and Δt is the computational time step.

The IBM force $\underline{f}$ in Eqn. (4b) is computed by: (1) *interpolation* of the prediction velocity $\underline{u}^*$ from the Eulerian to the Lagrangian grid, (2) *computation* of the force on the Lagrangian grid based on the difference between the interpolated velocity and the actual particle velocity and (3) *spreading* of this force from the Lagrangian to the Eulerian grid. The interpolation and spreading operations [5] are based on a regularized Dirac delta function δ_d that extends over 3 grid cells in all coordinate directions [6]. The scheme for computing the IBM force is summarized below:

$$\underline{U}^* (\underline{X}_l) = \sum_{ijk} \underline{u}^* (\underline{x}_{ijk}) \cdot \delta_d (\underline{x}_{ijk} - \underline{X}_l) \Delta x^3, \tag{5a}$$

$$\underline{F}^{n+1/2} (\underline{X}_l) = \frac{\underline{U}_d (\underline{X}_l) - \underline{U}^* (\underline{X}_l)}{\Delta t}, \tag{5b}$$

$$\underline{f}^{n+1/2} (\underline{x}_{ijk}) = \sum_{l} \underline{F}^{n+1/2} (\underline{X}_l) \cdot \delta_d (\underline{x}_{ijk} - \underline{X}_l) \Delta V_l \tag{5c}$$

Here the upper case letters refer to quantities defined on the Lagrangian grid, while the lower case letters denote quantities defined on the Eulerian grid. $\underline{x}_{ijk}$ denotes the position of the Eulerian grid point with index (i, j, k). $\underline{X}_l$ denotes the position of the Lagrangian grid point with index l. Δx is the grid spacing of the Eulerian grid. ΔV_l is the volume of the Lagrangian grid cells. It is determined from the requirements that its value is as close as possible equal to Δx^3 and that an integer number of Lagrangian grid points can be evenly distributed over the surface of a particle.

In Eqn. (5b) the force distribution is computed on the Lagrangian grid. From this the total force and torque acting on the particle can be determined. Substituting these expressions into Eqns

(3a)-(3b) yields [2]:

$$\rho_p V_c \frac{d\underline{u}_c}{dt} = -\rho_f \sum_l \underline{F}^{n+1/2}(\underline{X}_l)\,\Delta V_l + \rho_f \frac{d}{dt}\left(\int_V \underline{u}\,dV\right) + (\rho_p - \rho_f)\,V_c \underline{g}, \quad (6a)$$

$$I_c \frac{d\underline{\omega}_c}{dt} = -\rho_f \sum_l (\underline{X}_l - \underline{x}_c) \times \underline{F}^{n+1/2}(\underline{X}_l)\,\Delta V_l + \rho_f \frac{d}{dt}\left(\int_V [\underline{X} - \underline{x}_c] \times \underline{u}\,dV\right) \quad (6b)$$

Here the volume integrals are over the entire volume of the sphere and account for the inertia of the fluid in the space occupied by the sphere. It is remarked that for pressure-driven flows an additional force on the right-hand side of Eqn. (6a) must be included to account for the buoyant force from the associated background pressure stratification. From Eqns (6a)-(6b) the velocity of the centroid and the angular velocity of the sphere can be computed. Next, the desired particle velocity distribution $\underline{U}_d$ at the next time step can be calculated from Eqn. (2).

4. MODIFIED IBM

In a recent paper [1] I have shown that the method of Uhlmann [2] is approximately first-order accurate for Stokes flow through a regular array of *fixed* spheres. I have modified the method by implementing the multi-direct forcing scheme of Luo et al. [7] and by a slight retraction of the Lagrangian grid towards the interior of the sphere. It was shown that by these modifications the accuracy has drastically improved and second-order accuracy could be obtained [1]. Below the modifications to the original method are explained in more detail.

4.1 Multi-direct forcing scheme

Consider a particular Eulerian grid point (i,j,k) with velocity $\underline{u}^*$ close to the surface of a particle. After the interpolation and spreading steps, Eqns (5a) and (5c), a *diffuse* force distribution results that involves a lot more grid points than just this one particular grid point. Similarly, grid point (i,j,k) is involved in the forcing required for its neighbors. A consequence of this is that the resulting IBM force distribution will not exactly enforce the surrounding fluid to the desired particle velocity. Luo et al. [7] and Kriebitzsch et al. [8] proposed a *multi-direct forcing* scheme as a remedy for this problem. The idea is to iteratively determine the IBM forcing until the desired accuracy is achieved. In between Eqns (4b) and (4c) the following iterative scheme is included:

do $q = 1, N_q$

$$\underline{U}^{**}_{(q-1)} = \sum_{ijk} \underline{u}^{**}_{(q-1)} \delta_d \Delta x^3\,, \quad (7a)$$

$$\underline{F}^{n+1/2}_{(q)} = \underline{F}^{n+1/2}_{(q-1)} + \frac{\underline{U}_d - \underline{U}^{**}_{(q-1)}}{\Delta t}\,, \quad (7b)$$

$$\underline{f}^{n+1/2}_{(q)} = \sum_l \underline{F}^{n+1/2}_{(q)} \delta_d \Delta V_l\,, \quad (7c)$$

$$\underline{u}^{**}_{(q)} = \underline{u}^* + \Delta t\, \underline{f}^{n+1/2}_{(q)}\,, \quad (7d)$$

enddo

where N_q is the total number of iterations and $\underline{u}^{**}_{(0)}$ is the second prediction velocity as computed from Eqn. (4b). The original method of Uhlmann [2] corresponds to the case of $N_q = 0$. The value of N_q can be chosen at will, but for retaining the computational efficiency of the method it should preferably be kept low. Simulation results suggest that 2 iterations are optimal [1].

4.2 Retraction of Lagrangian grid

The use of the regularized Dirac delta function δ_d in the interpolation and spreading operations results in a diffuse particle interface *as seen by* the fluid phase. In fact, the interface of a particle is surrounded by a porous shell, which for the particular delta function of Roma et al. [6] has a width of three grid cells. Consequently, the effective particle diameter is larger than the actual particle diameter and this tends to an overestimation of the drag force experienced by the fluid. To correct for this the Lagrangian grid points are slightly retracted from the surface towards the interior of the particle with a *fraction* of the grid spacing Δx [1, 9, 10]. This is illustrated in Figure 2. I found that retraction has a strong influence on the accuracy of the IBM. Simulation results suggest that a retraction distance of $0.3\Delta x$ is close to optimal. For Stokes flow through a regular array of fixed spheres it was found that at this retraction value the method is second-order accurate. At a grid resolution of $2R/\Delta x = 16$ the error in the permeability of the array of spheres was about 1.5 %, almost 7 times smaller than the error of 9.8 % at zero retraction distance as in the original method of Uhlmann [1].

4.3 Direct account of fluid inertia within particle

For reasons of computational efficiency, Uhlmann [2] assumed rigid-body motion of the fluid inside the space occupied by the particles in order to simplify the volume integrals in Eqns (6a) and (6b). When this assumption holds, the second term on the right-hand side of Eqn. (6a) can be replaced by $\rho_f V_c d\underline{u}_c/dt$ and the second term on the right-hand of Eqn. (6b) by $(I_c/\rho_p) d\underline{\omega}_c/dt$. However, apart from a loss in accuracy associated with this assumption, this causes a singularity in the Newton-Euler equations for a density ratio $\rho_p/\rho_f \to 1$. It is for

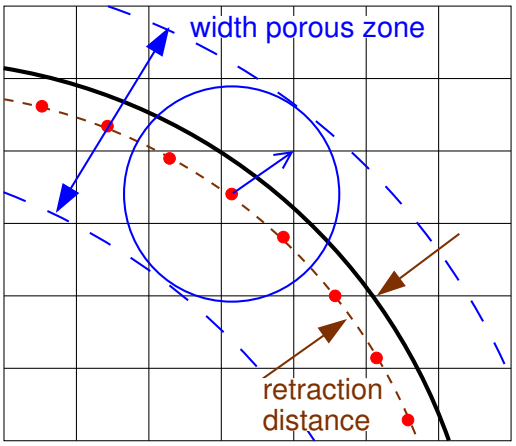

FIGURE 2. ILLUSTRATION OF THE RETRACTION DISTANCE. THE DOTS INDICATE THE POSITION OF THE LAGRANGIAN GRID POINTS, WHICH ARE RETRACTED FROM THE ACTUAL SURFACE (THE SOLID LINE) WITH A FRACTION OF THE EULERIAN GRID SPACING (ABOUT $0.3\Delta x$ IN THIS CASE). THE CIRCLE SHOWS THE EXTENT OF THE INTERPOLATION/SPREADING KERNEL AND IS INDICATIVE FOR THE WIDTH OF THE POROUS ZONE SURROUNDING THE PARTICLE'S SURFACE.

this reason that Uhlmann found that for spheres his method is only stable for density ratios larger than about 1.2 [2].

Kempe et al. [11] recognized the singularity problem caused by the assumption of rigid-body motion. They proposed to directly evaluate the volume integrals by means of a second-order accurate midpoint quadrature rule. For instance, the momentum integral in Eqn. (6a) is computed as:

$$\int_V \underline{u} dV = \sum_{ijk} \underline{u}\left(\underline{x}_{ijk}\right) \alpha_{ijk} \Delta x^3 . \tag{8}$$

Here α_{ijk} is the solid volume fraction of the particle in grid cell (i,j,k). Kempe et al. [11] determine α_{ijk} from a level-set function ϕ given by the signed distance to the particle surface ∂V with $\phi < 0$ inside and $\phi > 0$ outside the particle. The solid volume fraction is calculated from:

$$\alpha_{ijk} = \frac{\sum_{n=1}^{8} -\phi_n H\left(-\phi_n\right)}{\sum_{n=1}^{8} \|\phi_n\|} , \tag{9}$$

where the sum is over all 8 corner nodes of the grid cell volume and H is the Heaviside step function. Kempe et al. [11] validated the second-order accuracy as well as the computational efficiency of the above method.

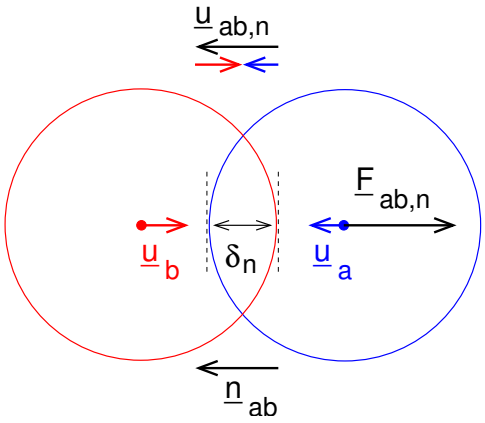

FIGURE 3. ILLUSTRATION OF THE SOFT-SPHERE MODEL FOR HEAD-ON COLLISION BETWEEN TWO EQUAL SPHERES.

I have implemented the above method in my IBM for direct evaluation of the volume integrals in the Newton-Euler equations. As shown by Kempe et al. [11], it is also my experience that the IBM is now stable for particle-fluid density ratios down to values much smaller than 1. Although not thoroughly investigated, it is expected that for very light particles the method will still become unstable as a result of the weak (explicit) coupling of the Navier-Stokes and Newton-Euler equations [12].

5. COLLISION MODEL

To model inter-particle and particle-wall contact forces, the present IBM is combined with a soft-sphere model [3]. The soft-sphere model is widely used in discrete particle models. In this model particles are allowed to slightly overlap with each other and the contact force is computed from the overlap between the particles and their relative velocity. The contact force is decomposed into a normal and a tangential component. The normal component of the contact force acting on particle a when in contact with particle b is parameterized as:

$$\underline{F}_{ab,n} = -k_n \delta_n \underline{n}_{ab} - \eta_n \underline{u}_{ab,n} , \tag{10}$$

where k_n is the normal spring stiffness, η_n is the normal damping coefficient, δ_n is the overlap between the particles, $\underline{n}_{ab}$ is the unit normal and $\underline{u}_{ab,n}$ is the relative velocity between the particles. The soft-sphere model is illustrated in Fig. 3 for a head-on collision between two equal spheres. In this paper no results are shown for tangential collisions, so therefore the discussion of the model is restricted to normal collisions only.

Input parameters of the soft-sphere collision model are the dry coefficient of restitution, e_d, and the time duration of a collision given as the number, N_c, of computational time steps. The coefficient of restitution, e, is defined as the change in the overlap at

the end of contact ($t = N_c\Delta t$) divided by the change in the overlap at the start of contact ($t = 0$):

$$e = -\frac{d\delta_n/dt|_{t=N_c\Delta t}}{d\delta_n/dt|_{t=0}}. \tag{11}$$

The *dry* coefficient of restitution is the coefficient of restitution for a collision where viscous dissipation of particle kinetic energy by the surrounding fluid can be neglected. The parameters k_n and η_n are related to e_d and $N_c\Delta t$ according to [3]:

$$k_n = \frac{m_e\left(\pi^2 + [\ln e_d]^2\right)}{[N_c\Delta t]^2}, \tag{12a}$$

$$\eta_n = -\frac{2m_e[\ln e_d]}{N_c\Delta t}, \tag{12b}$$

where $m_e = (1/m_a + 1/m_b)^{-1}$ is the effective mass of the two particles.

In the soft-sphere model the contact time ($N_c\Delta t$) is chosen much larger than the time predicted by Hertz contact theory [13] to avoid severe constraints on the numerical time step. However, with k_n and η_n given by Eqns (12a)-(12b) the model still yields the desired coefficient of restitution for dry collisions. As discussed by Van der Hoef et al. [3] the contact time should not be too large on the one hand to avoid severe overlapping between particles, but on the other hand it should not be too small in order to accurately resolve a collision in time. In the simulations shown in section 8 the contact time was fixed at $8\Delta t$ ($N_c = 8$).

6. NUMERICAL IMPLEMENTATION

Both the Navier-Stokes and the Newton-Euler equations are integrated in time with a third-order, three-step Runge-Kutta scheme [14], except for the pressure-gradient term in Eqn. (1b) for which the second-order Crank-Nicolson scheme is used. Conservation of mass of the fluid phase, Eqn. (1a), is enforced by a pressure-correction scheme similar to the scheme given by Eqns (4a)–(4e). This scheme is combined with the multi-direct forcing scheme given by Eqns (7a)–(7d) with the number of iterations fixed at $N_q = 2$. The retraction distance is fixed at $0.3\Delta x$. For the simulations shown in this paper, efficient, FFT-based, direct solvers could be used to compute the correction pressure from the associated Poisson equation. The Navier-Stokes equations are discretized on a uniform, staggered Cartesian grid with the finite-volume method in which spatial derivatives are obtained from the second-order central-differencing scheme.

As mentioned before, the coupling of the Navier-Stokes and the Newton-Euler equations is explicit/weak. Given the particle positions and velocities at time step n, first the Navier-Stokes equations are integrated to time step $n+1$ and then the Newton-Euler equations.

A few remarks about the numerical implementation of the soft-sphere model. The normal contact force is added as an extra force to the right-hand side of Eqn. (6a). The second-order Crank-Nicolson scheme is used to integrate this force in time. This scheme requires the contact force at time step $n+1$, which is iteratively determined as function of the particle positions and velocities at $n+1$ using under-relaxation with a relaxation factor of 0.5. The iterations are stopped until the changes in all particle positions are smaller than $10^{-5}\Delta x$. I have tested this scheme for the dry collision of a sphere onto a plane wall (with the lubrication force turned off): the computed value of the restitution coefficient (particle velocity at rebound divided by velocity at impact) is in excellent agreement with the model parameter e_d. The iterative scheme appears robust and convergence is fast; typically only a few iterations are needed. In case a particle collides with more than one particle at the same time, the contact forces are computed for each particle pair and added together componentwisely at each iteration.

The computational algorithm is coded in Fortran with the MPI extension for parallel execution on multi-processor machines with distributed memory. For the parallelization of the Navier-Stokes equations a standard domain-decompositioning technique is used, while for the particles I make use of a master-and-slave technique that is implemented in a similar fashion as described by Uhlmann [15].

7. RESULTS FROM LUBRICATION STUDY

In this section I explore the accuracy of the IBM for simulating the hydrodynamic interaction / lubrication between 2 equal spheres and the normal approach of a sphere towards a plane wall.

7.1 Normal approach between 2 equal spheres

Fig. 4 illustrates the flow field for the case of a normal approach between 2 spheres with equal radius and opposite velocity. The dimensions of the flow domain used for this simulation are $16R$ in the x and y-direction and $32R$ in the z-direction. Periodic boundary conditions are used in the z-direction, while in the x and y-direction free-slip and zero-pressure boundary conditions are imposed. Fig. 1 shows the Eulerian and Lagrangian grids used for this simulation. The resolution of the Eulerian grid is $2R/\Delta x = 16$, so the total number of Eulerian grid points is equal to $128x128x256 \approx 4.19 \cdot 10^6$. The number of Lagrangian grid points on the retracted surface of each sphere is 746 with the retraction distance set to $0.3\Delta x$. The particle Reynolds number, $Re_c \equiv \|\underline{u}_c\|2R/\nu_f$, is set to 0.1. For such low particle Reynolds number the flow field can be considered as quasi-steady. Therefore in all simulations discussed in this subsection the positions of the spheres are fixed and the sphere velocities are kept con-

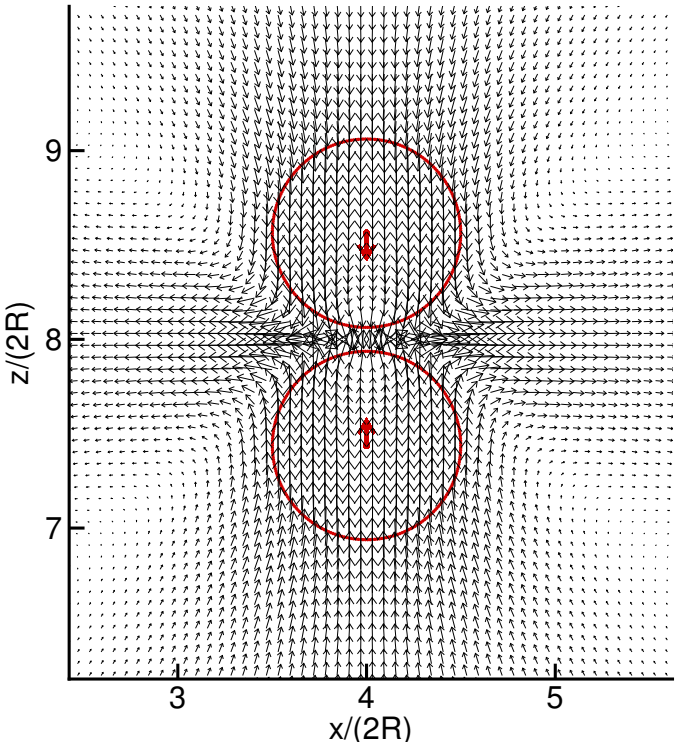

FIGURE 4. A CROSS-SECTION OF THE FLOW FIELD AT $Y = 0$ FOR THE CASE OF A NORMAL APPROACH BETWEEN 2 EQUAL SPHERES WITH RADIUS R AND OPPOSITE VELOCITY AT A PARTICLE REYNOLDS NUMBER $Re_c = 0.1$. THE GRID IS UNIFORM WITH RESOLUTION $2R/\Delta x = 16$. THE GAP WIDTH IN BETWEEN THE SPHERES IS EQUAL TO $0.25R$.

stant. Note that in this case the Newton-Euler equations do not need to be solved. Furthermore, after the initial transient the simulated flow field reaches a steady state. The computational time step is fixed at $\Delta t \|\underline{u}_c\|/(2R) = 0.5 \cdot 0.1375\, Re_c (\Delta x/2R)^2$ based on the diffusion criterion for numerical stability of the three-step Runge-Kutta scheme [16].

A series of simulations like shown in Fig. 4 has been conducted in which I varied the gap width between the spheres as well as the grid resolution. From the simulations the force on the spheres has been determined. It is convenient to write this force as $\underline{F} = -\lambda(\varepsilon) 6\pi\mu_f R \underline{u}_c$, where λ is the Stokes amplification factor that is a function of ε, the gap width between the spheres normalized by the radius of the spheres. The hydrodynamic interaction between the spheres vanishes for $\varepsilon \to \infty$ and thus in this limit $\lambda \to 1$; the force on each sphere is then equal to the Stokes drag experienced by a single sphere in free space. Brenner [17] derived an exact solution for λ as function of ε under the assumption that the flow is in the Stokes regime, that is for sufficiently

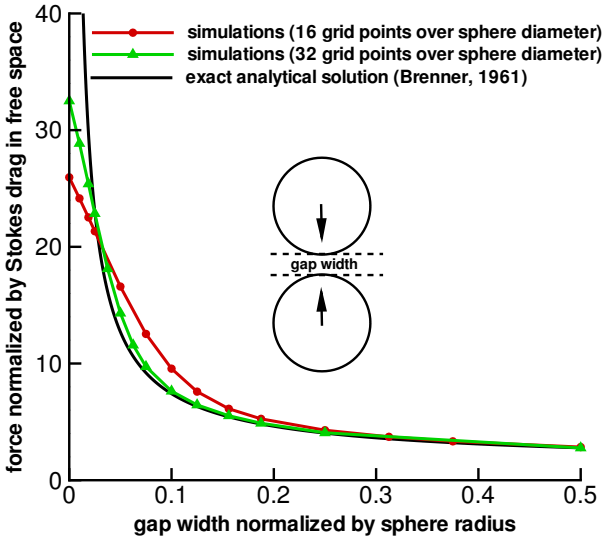

FIGURE 5. NORMALIZED FORCE ACTING ON 2 EQUAL SPHERES AT A NORMAL APPROACH WITH OPPOSITE VELOCITY AT A PARTICLE REYNOLDS NUMBER $Re_c = 0.1$, SHOWN AS FUNCTION OF THE NORMALIZED GAP WIDTH AND DIFFERENT GRID RESOLUTIONS.

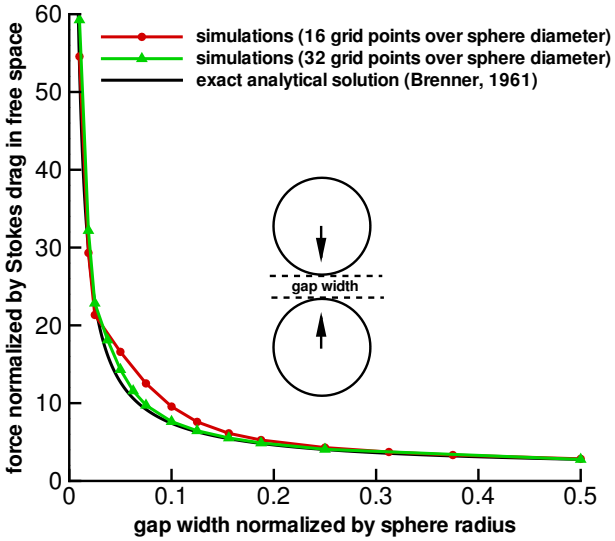

FIGURE 6. IDEM AS FOR FIG. 5, BUT WITH THE CORRECTION GIVEN BY EQNS (13a)-(13b) FOR $\varepsilon < \varepsilon_{ss}$.

low particle Reynolds number as in the present simulations. In Fig. 5 the simulation results for λ are compared against the exact solution over a range of ε. The simulated force is in close agreement with the exact solution for $\varepsilon \gtrsim 0.25$, which substantiates the accuracy of the IBM. For ε smaller than ≈ 0.25 the simulated force starts to deviate from the exact solution at resolution $2R/\Delta x = 16$, which at this resolution corresponds to a gap width smaller than 2 grid cells. Doubling the grid resolution to $2R/\Delta x = 32$ improves the simulated force, which at this resolution is in good agreement with the exact solution down to a gap width of $\varepsilon \approx 0.025$. This is quite remarkable since it corresponds to a gap width of $0.4\Delta x$, thus significantly smaller than Δx. For gap widths smaller than $\varepsilon \approx 0.025$, the drag force is underestimated in the simulations. This might also be expected since at such small gap widths the grid is too coarse to resolve the flow inside the gap. Refining the grid improves the estimate of the drag force somewhat, but not much. As a remedy I propose to add a correction term to the right-hand side of Eqn. (6a) to compensate for the error in the simulated drag force at very small gap widths [18, 19]. For simplicity this correction term is given here for the case of two equal spheres with *exactly opposite* velocity:

$$\Delta \underline{F}_{ss} = -6\pi\mu_f R \underline{u}_c \left[\lambda_{ss}(\varepsilon) - \lambda_{ss}(\varepsilon_{ss})\right], \qquad (13a)$$

where for both grid resolutions $\varepsilon_{ss} = 0.025$, which is the threshold value below which the correction term is turned on. $\lambda_{ss}(\varepsilon)$ is the asymptotic expansion of Brenner's exact solution accurate to $O(\varepsilon)$ [19]:

$$\lambda_{ss}(\varepsilon) = \frac{1}{2\varepsilon} - \frac{9}{20}\log\varepsilon - \frac{3}{56}\varepsilon\log\varepsilon + 1.346 + O(\varepsilon). \qquad (13b)$$

Fig. 6 shows the simulation results for the Stokes amplification factor including this asymptotic analytical correction for $\varepsilon < \varepsilon_{ss}$. In particular at resolution $2R/\Delta x = 32$, the corrected results are in good agreement with the exact solution over the whole range of ε.

7.2 Side-by-side approach of 2 equal spheres

Similar to Fig. 4, Fig. 7 illustrates the flow field for the case of a side-by-side approach of 2 equal spheres with opposite velocity and at a particle Reynolds number of $Re_c = 0.1$. Simulations have been executed for two different cases: the case of non-rotating spheres and the case of freely-rotating spheres with a net zero torque at steady state. Fig. 7 corresponds to the case of freely-rotating spheres at a gap width of $\varepsilon = 0.25$. The dimensions of the flow domain used for this simulation are $24R$ in the x and y-direction and $30R$ in the z-direction. Free-slip and zero-pressure boundary conditions are used in the x and z-direction, while periodic boundary conditions are imposed in

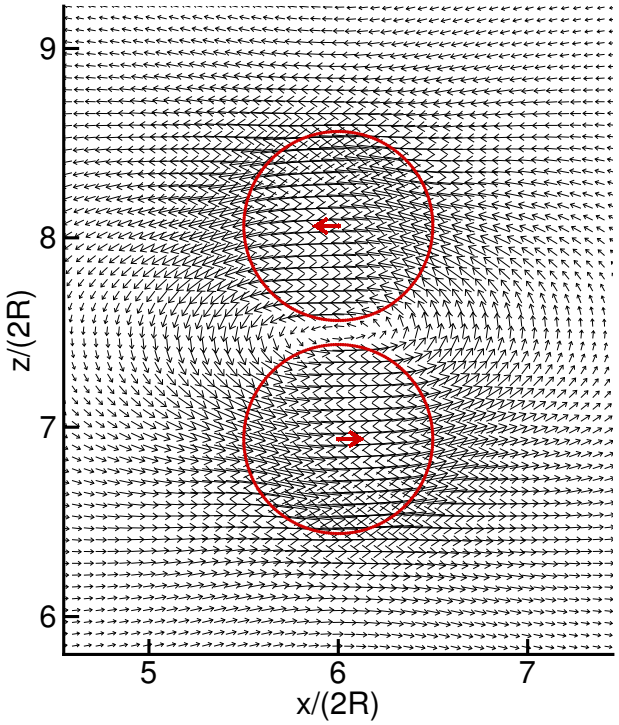

FIGURE 7. IDEM AS FOR FIG. 4, BUT NOW SHOWING THE SIDE-BY-SIDE APPROACH OF 2 EQUAL SPHERES WITH RADIUS R AND OPPOSITE CENTROID VELOCITY. THE SPHERES ROTATE FREELY.

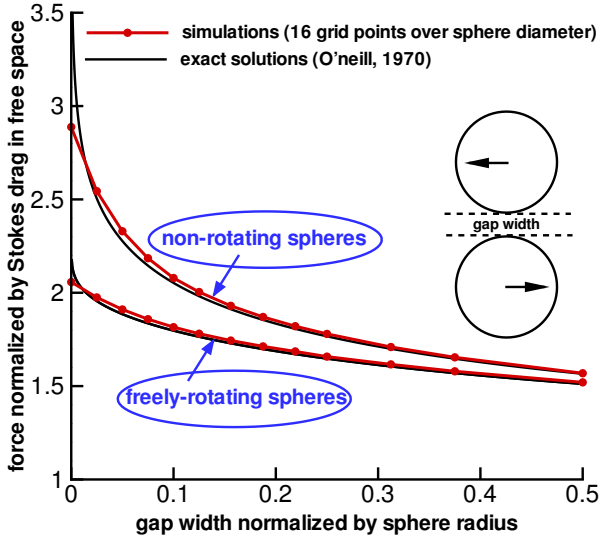

FIGURE 8. IDEM AS FOR FIG. 5, BUT NOW FOR THE CASE OF THE SIDE-BY-SIDE APPROACH OF 2 EQUAL SPHERES AND A GRID RESOLUTION $R/\Delta x = 16$ ONLY.

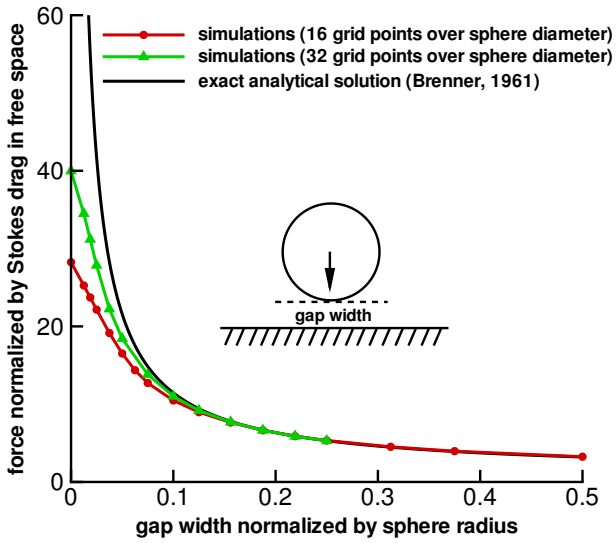

FIGURE 9. IDEM AS FOR FIG. 5, BUT NOW FOR THE CASE OF THE NORMAL APPROACH OF A SINGLE SPHERE TO A PLANE SOLID WALL.

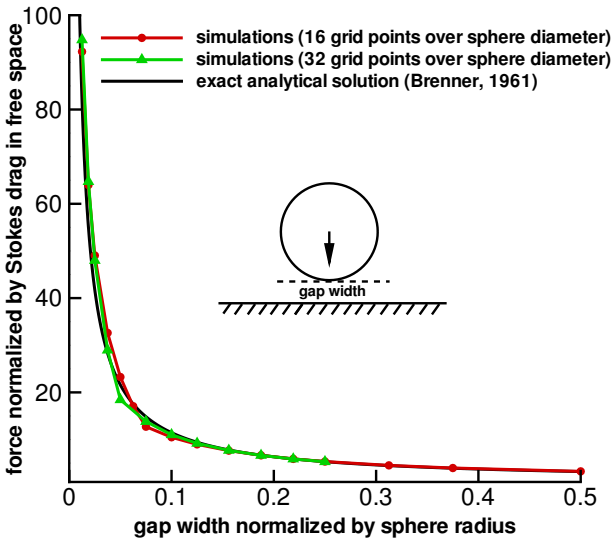

FIGURE 10. IDEM AS FOR FIG. 9, BUT WITH THE CORRECTION GIVEN BY EQNS (14a)-(14b) FOR $\varepsilon < \varepsilon_{sw}$.

the y-direction. The spheres are fixed in space and a constant sphere centroid velocity is imposed. In the case of freely-rotating spheres, the sphere angular velocity is determined from Eqn. (6b). All other simulation parameters are the same as for the case shown in Fig. 4.

A series of simulations like shown in Fig. 7 has been executed for both the non-rotating and the freely-rotating case. Fig. 8 depicts the Stokes amplification factor (λ) as a function of the normalized gap width (ε). The results are compared against the exact series solutions from O'Neill [20]. Interestingly, the simulated force on the spheres is in excellent agreement with the exact solutions for almost all ε. It is only for the non-rotating case that the results deviate at very small gap widths at which the exact solution for this case diverges to infinity. However, the more relevant case of freely-rotating spheres shows perfect agreement over the whole range up to zero gap width. It is remarked that in this case the analytical solution predicts that the force remains finite for $\varepsilon \to 0$; at zero gap width the velocity at the point of contact is equal to zero as the rotation of the spheres then exactly cancels their centroid velocity. The conclusion here is that the present IBM is capable of accurately simulating the side-by-side translation of 2 spheres. No corrections are needed for the realistic case in which they are allowed to rotate freely.

7.3 Normal approach of sphere towards plane wall

Similar to the case of a normal approach between 2 spheres, a series of simulations has been conducted of the normal approach of a sphere towards a plane wall. Again the particle Reynolds number is set to 0.1, so the flow is in the Stokes regime and can be considered as quasi-steady. The flow domain is a cube with dimension $16R$. Periodic boundary conditions are imposed in the lateral directions, free-slip and zero-pressure boundary conditions at the top boundary and no-slip boundary conditions on the wall at the bottom boundary. Fig. 9 shows the simulated force (λ) as a function of the gap width (ε). The results are compared against the exact solution derived by Brenner [17]. Excellent agreement with the analytical solution is found for a gap width of $\varepsilon \gtrsim 0.1$. As expected, the simulations underestimate the drag force for very small gap width. The higher the grid resolution, the smaller the error. Similar to the case of a normal approach between 2 spheres, I have implemented a correction term on the right-hand side of Eqn. (6a) to compensate for the error in the force on a sphere approaching a plane wall:

$$\Delta \underline{F}_{sw} = -6\pi\mu_f R \underline{u}_c \left[\lambda_{sw}(\varepsilon) - \lambda_{sw}(\varepsilon_{sw})\right], \qquad (14a)$$

where $\varepsilon_{sw} = 0.075$ at $2R/\Delta x = 16$ and $\varepsilon_{sw} = 0.05$ at $2R/\Delta x = 32$ with ε_{sw} the threshold value below which the correction term is turned on. $\lambda_{sw}(\varepsilon)$ is the asymptotic expansion of Brenner's exact

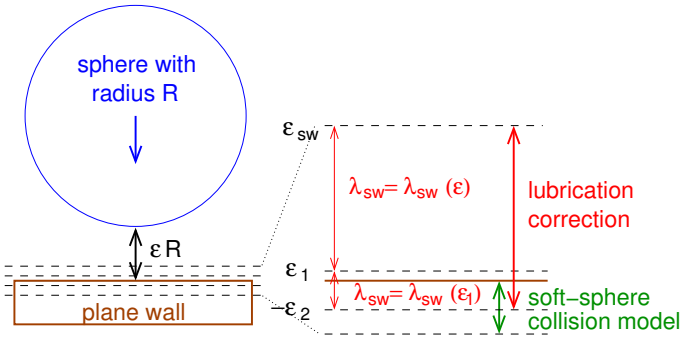

FIGURE 11. ILLUSTRATION OF THE COMBINED LUBRICATION / SOFT-SPHERE MODEL FOR THE COLLISION OF A SPHERE ONTO A PLANE SOLID WALL.

solution accurate to $O(\varepsilon)$ [21]:

$$\lambda_{sw}(\varepsilon) = \frac{1}{\varepsilon} - \frac{1}{5}\log\varepsilon - \frac{1}{21}\varepsilon\log\varepsilon + 0.9713 + O(\varepsilon). \quad (14b)$$

Fig. 10 shows the simulation results for the Stokes amplification factor including this asymptotic analytical correction for $\varepsilon < \varepsilon_{sw}$. For both resolutions the corrected results are in good agreement with the exact solution over the whole range of ε.
The case of a sphere moving parallel to a plane wall has not yet been investigated in detail. However, similar to the case of the side-by-side motion of 2 spheres, it is anticipated that the present IBM is accurate down to very small gap width and therefore that this case does not require any corrections to the method.

8. RESULTS FROM COLLISION STUDY

Fig. 11 illustrates how the soft-sphere model is implemented into the present IBM and combined with the lubrication force corrections discussed in the previous section. Considering the case of a sphere-wall collision, the lubrication force correction given by Eqn. (14a) is switched on when the gap width becomes smaller than $\varepsilon_{sw}R$. Note that the lubrication force correction holds for the case of *fully rigid / inelastic* particles, which do not deform and for which the Stokes amplification factor diverges to infinity for $\varepsilon \to 1$. When this would be true the particle would never touch (nor rebound at) the wall and would come to halt at finite gap width. However, for a particle and wall that are allowed to deform, the Stokes amplification factor will remain finite. Furthermore, surface roughness effects come into play at gap widths on the order of the typical roughness height [22] and in this regime the lubrication force correction loses its validity. To accomodate actual contact in the present collision model, the Stokes amplification factor is fixed to a constant value $\lambda_{sw} = \lambda_{sw}(\varepsilon_1)$ when the gap width becomes smaller than a specified threshold value of $\varepsilon_1 R$. For $\varepsilon < 0$ the particle is in contact with the wall and the soft-sphere model becomes active. To avoid excessive energy dissipation by the lubrication force correction during contact time (which is arbitrarily set in the soft-sphere model), the lubrication force correction is turned off for an overlap between particle and wall larger than $\varepsilon_2 R$. The threshold values ε_1 and ε_2 have to be determined from test simulations such as discussed below.
In this section simulation results are shown for the gravity-driven *wet* collision of a sphere onto a plane wall. The collision is called *wet* for it takes place in a viscous fluid and as a consequence part of the particle kinetic energy is dissipated by the fluid during collision. The coefficient of restitution for wet collisions is thus smaller than for a dry collision. According to the elastohydrodynamic collision theory of Davis et al. [23], the coefficient of restitution of wet collisions is primarily determined by the Stokes number. This number is a measure for the change in the particle inertia by the viscous drag force from the surrounding fluid:

$$St = \frac{\rho_p V_c \|\underline{u}_c\|}{6\pi\mu_f R^2}. \quad (15)$$

Legendre et al. [24] assembled data from many different experiments on the bouncing of *both* drops and solid particles on a plane wall. Interestingly, the experimental results for the coefficient of restitution scatter around a curve given by:

$$e/e_d = \exp(-35/St). \quad (16)$$

A series of simulations has been carried out to test whether the combined IBM / soft-sphere collision model is capable of reproducing the experimental results. A steel sphere with radius R is released in a closed rectangular box filled with RV20 silicone oil. In the simulations the sphere radius is varied from $R = 0.625 \cdot 10^{-3}$m till $R = 2.75 \cdot 10^{-3}$m. The dimensions of the rectangular box are 24 radii in the horizontal directions and 48 radii in the vertical direction. At release the centroid of the sphere is positioned in the center of the box at 1,5 radii from the top wall. The mass density of the silicone oil is 953 kg·m^{-3} and the kinematic viscosity of the oil is equal to $2.1 \cdot 10^{-5}$ m^{2}s^{-1}. The steel / oil mass density ratio is 8.18. The gravitational acceleration is 9.81 ms^{-2}. The grid resolution in the simulations is $2R/\Delta x = 16$ and the retraction distance is $0.3\Delta x$. The following values for the collision parameters are used: (1) the dry coefficient of restitution is set to 0.97; (2) the collision contact time is fixed at $8\Delta t$ with Δt equal to half the maximum allowed time step for stability of the Runge-Kutta scheme [16]; (3) $\varepsilon_1 = 10^{-3}$ and $\varepsilon_2 = 10^{-2}$.
From the simulations the restitution coefficient is computed as the ratio of the maximum velocity at the end of collision contact

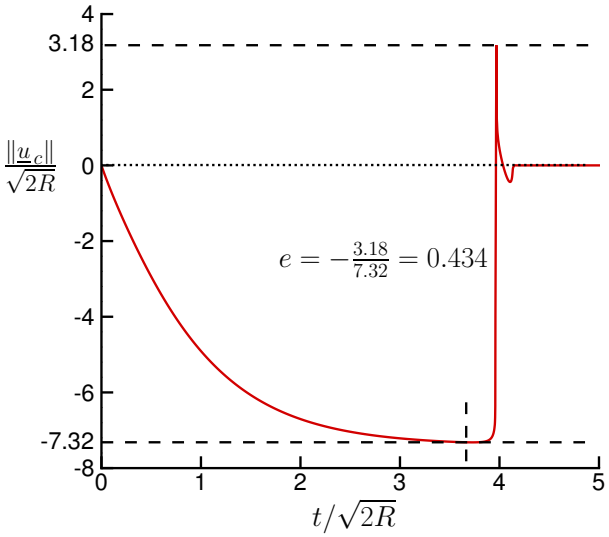

FIGURE 12. NORMALIZED CENTROID VELOCITY AS FUNCTION OF NORMALIZED TIME OF A STEEL SPHERE FALLING IN SILOCONE OIL ONTO A PLANE WALL. THE SPHERE RADIUS IS EQUAL TO $R = 1.25 \cdot 10^{-3}$M.

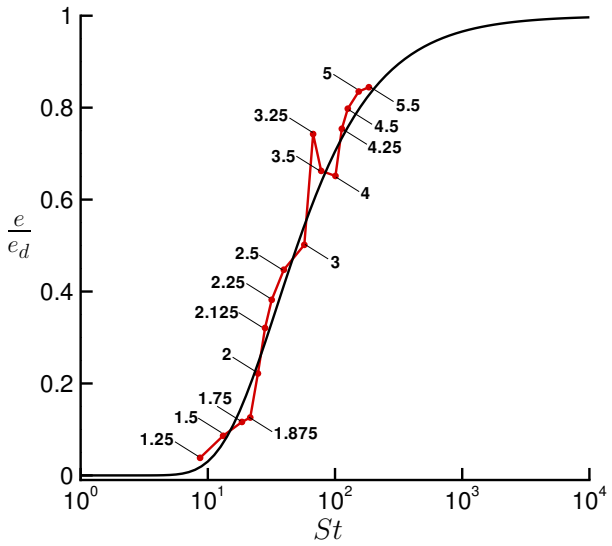

FIGURE 13. NUMERICAL RESULTS FOR THE RESTITUTION COEFFICIENT OF A STEEL SPHERE IN SILICONE OIL AT FIRST IMPACT ON A PLANE WALL. THE COEFFICIENT IS NORMALIZED WITH THE DRY COEFFICIENT OF RESTITUTION AND SHOWN AS FUNCTION OF STOKES NUMBER BASED ON THE SPHERE IMPACT VELOCITY. THE NUMBERS REFER TO THE SPHERE DIAMETERS (IN MM) USED IN THE SIMULATIONS. THE BLACK SOLID LINE IS A FIT FROM EXPERIMENTAL DATA GIVEN BY EQN. (16).

to the maximum velocity just prior to collision impact. Fig. 12 illustrates this definition of the restitution coefficient for the simulation in which the sphere radius is equal to $R = 1.25 \cdot 10^{-3}$m. Fig. 13 depicts the ratio e/e_d at first rebound as function of the Stokes number together with the experimental fit given by Eqn. (16). The Stokes number is based on the maximum velocity just prior to impact. The agreement between the simulations and the experiments is good over the whole range of Stokes numbers, in particular when considering the scatter in the experimental data. For a Stokes number smaller than about 10, the coefficient of restitution becomes almost zero and the sphere does not detach from the wall after impact.

The numerical results are sensitive to the choice of the collision parameters ε_1 and ε_2. Numerous test simulations were carried out to determine which values are appropriate; the results shown in Fig. 13 are for values of ε_1 and ε_2 for which the agreement is good. It is planned to investigate in more detail how these values are related to the other collision model parameters, in particular the collision contact time. Nonetheless, the conclusion that can be drawn here is that with the appropriate choice of the collision parameters the combined IBM / soft-sphere collision model indeed captures the observed behavior in the experiments.

9. MAIN CONCLUSIONS

A combined IBM / soft-sphere collision model has been developed. In a lubrication study the hydrodynamic interaction has been studied between non-touching particles at close distance from each other. The numerical results for the drag force acting on the particles agree well with exact analytical solutions, except for a gap width between the particles that is significantly smaller than the numerical grid spacing. For such very small gap widths, lubrication force corrections are incorporated in the model for the normal approach between two particles and for the normal approach of a particle towards a wall. Results have been shown from a numerical study of sphere-wall collisions in a viscous fluid. The simulated behavior of the coefficient of restitution as function of the Stokes number based on the particle impact velocity, is in good agreement with experimental data.

REFERENCES

[1] Breugem, W.-P., and Boersma, B. J., 2010. "Direct numerical simulation of turbulent flows laden with finite-size particles". In Proceedings of the 8th International ERCOF-

TAC Symposium on Engineering Turbulence, Modelling and Measurements (ETMM8, Marseille, France, 9–11 June 2010). Paper number 87.

[2] Uhlmann, M., 2005. "An immersed boundary method with direct forcing for the simulation of particulate flows". *J. Comp. Phys.,* ***209***, pp. 448–476.

[3] Van der Hoef, M. A., Ye, M., Van Sint Annaland, M., Andrews IV, A. T., Sundaresan, S., and Kuipers, J. A. M., 2006. "Multi-scale modeling of gas-fluidized beds". *Adv. Chem. Engng,* ***31***, pp. 65–149.

[4] Mittal, R., and Iaccarino, G., 2005. "Immersed boundary methods". *Ann. Rev. Fluid Mech.,* ***37***, pp. 239–261.

[5] Peskin, C. S., 2002. "The immersed boundary method". *Acta Numerica,* ***11***, pp. 479–517.

[6] Roma, A. M., Peskin, C. S., and Berger, M. J., 1999. "An adaptive version of the immersed boundary method". *J. Comp. Phys.,* ***153***, pp. 509–534.

[7] Luo, K., Wang, Z., Fan, J., and Cen, K., 2007. "Full-scale solutions to particle-laden flows: Multidirect forcing and immersed boundary method". *Phys. Rev. E,* ***76***(066709).

[8] Kriebitzsch, S., Van der Hoef, M., and Kuipers, H., 2010. "Direct numerical simulations of gas-particle flows using an immersed boundary method". In Proceedings of the Academy Colloquium Immersed Boundary Methods: Current Status and Future Research Directions (KNAW, Amsterdam, The Netherlands, 15–17 June 2009).

[9] Höfler, K., and Schwarzer, S., 2000. "Navier-Stokes simulation with constraint forces: finite-difference method for particle-laden flows and complex geometries". *Phys. Rev. E,* ***61***(6), pp. 7146–7160.

[10] Yu, Z., and Shao, X., 2007. "A direct-forcing fictitious domain method for particulate flows". *J. Comp. Phys.,* ***227***, pp. 292–314.

[11] Kempe, T., Schwarz, S., and Fröhlich, J., 2010. "Modelling of spheroidal particles in viscous flows". In Proceedings of the Academy Colloquium Immersed Boundary Methods: Current Status and Future Research Directions (KNAW, Amsterdam, The Netherlands, 15–17 June 2009).

[12] Hu, H. H., Patankar, N. A., and Zhu, M. Y., 2001. "Direct numerical simulations of fluid-solid systems using the arbitrary Lagrangian-Eulerian technique". *J. Comp. Phys.,* ***169***, pp. 427–462.

[13] Johnson, K. L., 1985. *Contact mechanics*. Cambridge University Press, United Kingdom.

[14] Spalart, P. R., Moser, R. D., and Rogers, M. M., 1991. "Spectral methods for the Navier-Stokes equations with one infinite and two periodic directions". *J. Comp. Phys.,* ***96***(2), pp. 297–324.

[15] Uhlmann, M., 2003. Simulation of particulate flows on multi-processor machines with distributed memory. Technical Report No. 1039, CIEMAT, Madrid (Spain), ISSN 1135-9420.

[16] Wesseling, P., 2001. *Principles of computational fluid dynamics*. Springer series in computational mathematics, Vol. 29, Springer-Verlag, Berlin.

[17] Brenner, H., 1961. "The slow motion of a sphere through a viscous fluid towards a plane surface". *Chem. Eng. Sci.,* ***16***, pp. 242–251.

[18] Ladd, A. J. C., and Verberg, R., 2001. "Lattice-Boltzmann simulations of particle-fluid suspensions". *J. Stat. Phys.,* ***104***, pp. 1191–1251.

[19] Dance, S. L., and Maxey, M. R., 2003. "Incorporation of lubrication effects into the force-coupling method for particulate two-phase flows". *J. Comp. Phys.,* ***189***, pp. 212–238.

[20] O'Neill, M. E., 1970. "Exact solutions of the equations of slow viscous flow generated by the asymmetrical motion of two equal spheres". *Appl. Sci. Res.,* ***21***, pp. 452–465.

[21] Jeffrey, D. J., 1982. "Low-Reynolds-number flow between converging spheres". *Mathematika,* ***29***, pp. 58–66.

[22] Joseph, G. G., Zenit, R., Hunt, M. L., and Rosenwinkel, A. M., 2006. "Particle-wall collisions in a viscous fluid". *J. Fluid Mech.,* ***443***, pp. 329–346.

[23] Davis, R. H., Serayssol, J.-M., and Hinch, E. J., 1986. "The elastohydrodynamic collision of two spheres". *J. Fluid Mech.,* ***163***, pp. 479–497.

[24] Legendre, D., Zenit, R., Daniel, C., and Guiraud, P., 2006. "A note on the modelling of the bouncing of spherical droplets or solid spheres on a wall in viscous fluid". *Chem. Eng. Sci.,* ***61***, pp. 3543–3649.